KRONOS FUSION ENERGY

PAPER 2.100 · THE KRONOS 2026 SERIES

Lifetime-Constrained Operating-Window Synthesis for a Compact Spherical-Tokamak Breeder: The Source-Strength-Centrepost-Life Trade and the Admissible Current Window

A breeder's operating point is not chosen freely; it is boxed in by competing mission and lifetime constraints, and the shape of that box — its floors, its ceilings, and which of...

Read it live — 3-D model · physics validator · film series

BY P I FORDOFFICIAL VERSION: HTTPS://WWW.KRONOSFUSIONENERGY.COM/PUBLICATIONS/ADMISSIBLE-OPERATING-WINDOW-SYNTHESIS.HTML AND G L KULCINSKI

2026 · EDITORIAL EDITION

THE OFFICIAL RECORD

What this document is, and how to read its numbers

This is a combined editorial. It gathers, in one volume, the two design studies Kronos Fusion Energy released in 2026 — a compact spherical-tokamak tritium/helium-3 breeder and a deuterium–helium-3 tandem-mirror generator — together with the intellectual-property estate, the people, and, in the internal edition, the full commercial case. The scientific text is the same text that appears in the arXiv preprints and the journal submissions; the editorial adds the apparatus a reader needs to hold the whole program at once, and nothing in the physics is altered to fit it.

THE HONESTY STANCE IS THE ASSET

Every headline quantity carries an **evidence class** — DERIVED RECOMPUTED MEASURED REQUIREMENT — and, where a number is a modelled extrapolation rather than a demonstrated value, it is labelled as such and its downside is shown next to it. Several quantities in the underlying corpus moved after first publication; where a value has been withdrawn or restated, the record says so plainly. This is deliberate: a diligence team will find the load-bearing assumptions, so the document surfaces them first.

TWO EDITIONS

This volume is issued in two editions. The **public edition** (light) carries the physics and the design only — no dollar, price, or per-kilogram figure appears anywhere in it. The **internal edition** (dark) adds the economics, the funding architecture, and the defense-commercial analysis, and is marked *Confidential* accordingly; it is not for public distribution. Where the commercial case rests on a modelled assumption rather than a demonstrated one, it is labelled as such and its downside is shown alongside it, on the same terms as the physics.

TITLE	The Kronos Fleet — Hyperion · Aegis · MetroVolt: A Combined Design & Commercialization Study
AUTHOR	Priyanca Ford, Founder & CEO, on behalf of Kronos Fusion Energy
EDITION	2026 Combined Editorial · first issue
COMPANION WORKS	The five-paper arXiv drop — (1) Breeder, (2) Burner, (3) REBCO magnet & tape, (4) Direct Energy Conversion, (5) AI/ML/Quantum control — with matching numbered Zenodo deposits, plus the IOP journal and IAEA-FEC submissions. Patents were filed before the drop.
NAMING	Hyperion = the breeder; Aegis (defense) and MetroVolt (data-center) = one generator in two housings. Internal mode letters (D1, L) do not appear on public surfaces.
STATUS	Conceptual design & simulation study. Nothing herein is a construction commitment.

HOW TO READ THIS VOLUME

The fleet at a glance, and the way its numbers are marked

This volume opens with *Orientation*, presents the five research papers as a bound sequence, and closes with the *Apparatus*. *Foundations* sets out the three general results both machines rest on. *Paper One* is the Hyperion breeder; *Paper Two* the Aegis / MetroVolt generator; *Papers Three, Four and Five* are the enabling science — high-field REBCO magnets and tape, direct energy conversion, and the AI / ML / quantum control stack. A *Digital Twin & 3-D Model* part follows, then the *Environmental* profile. The *Economics* and levelized cost and the *Business Case* and diligence record appear in the internal edition only; the *Simulations* proof record and the Apparatus — patent portfolio, team, limitations, and sources — close both editions.

THE FLEET AT A GLANCE

	HYPERION	AEGIS	METROVOLT
Role	Strategic-isotope foundry	Defense installation power	Campus power
Machine	**Spherical tokamak**	**Tandem mirror**	**Tandem mirror**
Fuel	Deuterium–tritium	Deuterium–helium-3	Deuterium–helium-3
Delivers	Tritium · ^{3}He · 14 MeV n	Resilient installation power	Firm campus power
Physics bar	**Fusion gain only**	Closure (gates named)	Closure + lunar ^{3}He
In the fleet	Breeds the fuel	Proves the generator	Commercial destination

HOW THE NUMBERS ARE MARKED

Every headline quantity carries an evidence class — DERIVED from first principles, RECOMPUTED from raw data, MEASURED in hardware, or a REQUIREMENT yet to be met. Financial figures carry a case label and are confined to the internal (confidential) edition. Values that moved after first publication are shown as withdrawn or restated rather than quietly changed. A capability you can evaluate is one whose limits are on the page.

ABSTRACT

Lifetime-Constrained Operating-Window Synthesis for a Compact Spherical-Tokamak Breeder: The Source-Strength-Centrepost-Life Trade and the Admissible Current Window

A breeder's operating point is not chosen freely; it is boxed in by competing mission and lifetime constraints, and the shape of that box — its floors, its ceilings, and which of them actually bind — is a design result in its own right. We synthesise the admissible operating window of the Hyperion compact spherical-tokamak breeder (design point $I_p = 9.656$ MA, $Q = 3.076$, $P_{\text{fus}} = 85.04\,MW$, negative triangularity $\delta = -0.30$, $B_0 = 8\,T$, elongation $\kappa = 2.0$, major radius $R_0 = 1.20\,m$, aspect ratio $A = 2.5$, centrepost peak field $16.84\,T$) from two frozen findings, and we derive both as governing equations rather than assert them. First, a strict invariance: because the first-wall load and the centrepost fast-neutron flux are driven by the same 14 MeV source, the neutron source strength S_n and the centrepost life τ_{life} obey $S_n\,\tau_{\text{life}} \lesssim \Psi_{\text{cp}}$ with Ψ_{cp} a device constant — a fixed per-cartridge neutron budget, so there is *no free operating-point gain*: buying more source strength always spends centrepost life in a fixed ratio, and the swap cadence rises linearly with S_n. We show the design runs at $\tau_{\text{life}} \approx 0.21$ fpy (~ 4.9 swaps fpy^{-1}) and mid-current at ≈ 0.46 fpy, exactly as the invariance predicts. Second, the admissible plasma current is a coupled floor/ceiling feasibility problem $I_p \in [I_{\min}, I_{\max}] = \bigcap_k \{I_p : g_k(I_p) \geq 0\}$, which we recast as a control-barrier-certified safe set. The floor $I_{\min} = 8.779$ MA is the q_{95}/ideal-MHD edge ($q_{95} \leq 3.3$ of the validated band); the ceiling $I_{\max} = 9.656$ MA is co-set by the centrepost fluence (≤ 18.85 dpa fpy^{-1}) and the ideal-kink margin ($q_{95} \geq 2.7$). The design current sits at that ceiling: the machine is deliberately run as hard as the consumable centrepost allows. The tritium-startup requirement, usually assumed binding, is non-binding throughout — $3.17 > 1.87$ kg yr^{-1}, a $1.70\times$ margin. All results were produced by the NVIDIA GPU HPC campaign (reduced-order power balance, OpenMC neutronics, free-boundary Grad–Shafranov, and gyrokinetic transport) and every headline number is a frozen anchor in the Kronos de-risking register. The contribution is a systems/constraint-synthesis result that names the box and the binding gates, distinct from the structural, fuel-cycle and design-scan papers of the series.

Open-access deposit (code & data, CC BY 4.0): DOI 10.5281/zenodo.22645799 · Zenodo community *kronos_fusion_energy*. Explore it live: interactive 3-D model · physics validator.

Keywords: operating window · source-strength invariance · centrepost life · plasma current · edge safety factor · control-barrier function · negative triangularity · spherical-tokamak breeder

CONTENTS

Table of Contents

NOMENCLATURE

Symbols, units, and the names of things

Q	plasma (fusion) gain, P_{fus}/P_{aux}
Q_E	engineering gain, net electric out / recirculating in
H_{98}	confinement enhancement over the IPB98(y,2) scaling
Z_{eff}	effective ion charge
c_{ee}	electron–electron bremsstrahlung leading coefficient, 2.120022 (exact)
τ_E	energy confinement time
I_p	plasma current
R_0, a	major radius, minor radius
κ, δ	elongation, triangularity
β_N	normalized plasma beta (Troyon-normalized)
TBR	tritium breeding ratio
DEC	direct energy conversion
CF	plant capacity factor (availability)
FOAK / NOAK / BOAK	first / nth / best of a kind
Hyperion	the ST breeder (internal: Mode D2)
Aegis	the generator, defense/installation housing (internal: Mode M)
MetroVolt	the generator, data-center housing (Mode M)

§ 1

Introduction

WHERE A BREEDER IS ALLOWED TO OPERATE

Where a fusion breeder operates is decided by the constraints that box it in, not by a single figure of merit. For a compact, high-power-density spherical tokamak (ST) the box is unusually tight. The ST confines a large plasma current in a small volume, which is precisely what makes it an attractive 14 MeV neutron source and breeding platform [1,2,3,4], and at the same time forces the inboard leg of the toroidal-field magnet — the centrepost — into a radial space so narrow that it cannot carry a reactor-lifetime neutron shield. The centrepost therefore accumulates fast-neutron fluence quickly and becomes a *consumable*: a scheduled-replacement cartridge rather than a permanent structure. Once that design choice is made, the operating point is no longer a free optimisation. Every increment of neutron source strength that the mission wants is paid for in centrepost life, and the plasma current that sets the source strength is simultaneously bounded below by edge stability and above by fluence. Making the resulting box explicit is the subject of this paper.

PRIOR ART

The individual walls of the box are each grounded in a mature literature. The upper bound on plasma current through the edge safety factor and the ideal external kink is classical tokamak stability [6,7,8,9]; the operational density limit is the Greenwald scaling [10]; the β ceiling is the Troyon limit [6]; and free-boundary equilibrium reconstruction with real-time q_{95} and shape is standard practice [12,13]. On the nuclear side, neutron damage (displacements-per-atom, dpa), transmutation and component lifetime in a fusion first wall are well characterised [14,15], and the sensitivity of REBCO coated conductor to fast-neutron fluence is an active materials question [16]. The consumable-centrepost idea itself descends from the demountable-magnet compact-tokamak line [4,5] and from the spherical-torus neutron-source concepts [1,3]. What is missing, and what a builder actually needs, is the *synthesis*: a single statement of the admissible operating window that (i) derives the trade between source strength and centrepost life as an invariance rather than a scan artifact, (ii) writes the current-window bounds as constraint functions and identifies which of them bind, and (iii) does so at the frozen design point of a specific machine so that every number is auditable.

CONTRIBUTION

This paper contributes exactly that synthesis for the Hyperion breeder. We give: a governing-equations treatment of the neutron source-strength model and the fluence–life relation, from which the source-strength/centrepost-life invariance follows in closed form (§2); a formal statement of the admissible current window as a constraint-intersection feasibility problem, recast as a control-barrier-function (CBF) safe set with a provable forward-invariance guarantee (§2.4); a description of the NVIDIA GPU HPC campaign — the reduced-order power-balance solver, the OpenMC neutron-transport model, the free-boundary Grad–Shafranov solver and the gyrokinetic transport codes — that produced every number, with its discretisation, solvers and convergence (§3); a results section with nine data figures and four tables (§4); a quantitative discussion against the published ST, density-limit, β-limit and materials benchmarks (§5); one honest open gate (§6); and a conclusion (§7). Every quantitative claim traces to a frozen serial in the Kronos Physics De-Risking Register [29] (gates BR-L1-A2, BR-L1-A7, BR-L1-A13, KX-L1-A21 and companions), cited inline so each is checkable. The finding sits inside a locked 115-paper series: the confinement basis that underwrites the operating point is the negative-triangularity turbulence result cross-validated by two gyrokinetic codes [32]; the consumable centrepost it lives on is developed in the remaining-useful-life prognostics paper [33], the swap-logistics and radial-budget-reconciliation paper [34], and the fleet-availability study [35]; the headroom in the constraints that do *not* bind here is red-teamed in [36]; the platform context is [30]; and the verification discipline behind the frozen anchors is [31].

§ 2

Governing equations and the formal problem

THE NEUTRON SOURCE-STRENGTH MODEL

For a deuterium–tritium plasma with electron density n_e, a 50:50 fuel mix ($n_D = n_T = \frac{1}{2} n_e$, ignoring dilution to leading order) and ion temperature T_i, the volumetric fusion reaction-rate density is $\frac{1}{4} n_e^2 \langle\sigma v\rangle(T_i)$, with $\langle\sigma v\rangle$ the Maxwellian-averaged D–T reactivity of Bosch and Hale [11]. The total 14 MeV neutron source strength is the volume integral

$$S_n = \int_V \tfrac{1}{4}\, n_e^2(\quad r)\,\langle\sigma v\rangle\big(T_i(\quad r)\big)\,\mathrm{d}V = \tfrac{1}{4}\, g_p\, \bar{n}_e^2\, \langle\sigma v\rangle(\bar{T}_i)\, V,$$

where over-bars are volume averages and $g_p = \overline{n_e^2 \langle\sigma v\rangle} / (\bar{n}_e^2 \langle\sigma v\rangle(\bar{T}_i))$ is an $O(1)$ profile-peaking factor. The line-averaged density is parametrised by the Greenwald fraction [10],

$$\bar{n}_e = f_G\, n_{\mathrm{GW}}, \qquad n_{\mathrm{GW}} = \frac{I_p\,[\mathrm{MA}]}{\pi a^2} \times 10^{20}\ \mathrm{m}^{-3},$$

with minor radius $a = R_0/A = 0.48\,m$. Substituting (2) into (1) and holding the fixed geometry (a, V) gives the source-strength scaling that the whole window turns on,

$$\boxed{S_n \;=\; \kappa_S\, f_G^2\, I_p^2\, \langle\sigma v\rangle(\bar{T}_i)}\,, \qquad \kappa_S = \frac{g_p\, V}{4} \left(\frac{10^{20}}{\pi a^2}\right)^2.$$

Near the operating temperature the D–T reactivity is close to a power law, $\langle\sigma v\rangle \propto T_i^{\ \nu}$ with $\nu \approx 2$ over 10–20 keV, so along a locus of fixed f_G and T_i the source strength scales as $S_n \propto I_p^\beta$ with $\beta \approx 2$, the exponent that the register reproduces (BR-L1-A2). At the frozen design point equation (3) evaluates to $S_n = 3.009 \times 10^{19}\ \mathrm{n\,s^{-1}}$ (BR-L1-A2), which is the neutron power $P_n = S_n E_n = 67.8\,MW$ at $E_n = 14.06\,MeV$ and hence $P_{\mathrm{fus}} = P_n/0.80 = 85.04\,MW$, the frozen fusion power. The reactivity model and the resulting iso-source contours of the (f_G, T_i) plane are shown in figure 1; the register operating points (design, off-duty peak, and a low-temperature high-Q point) are overlaid.

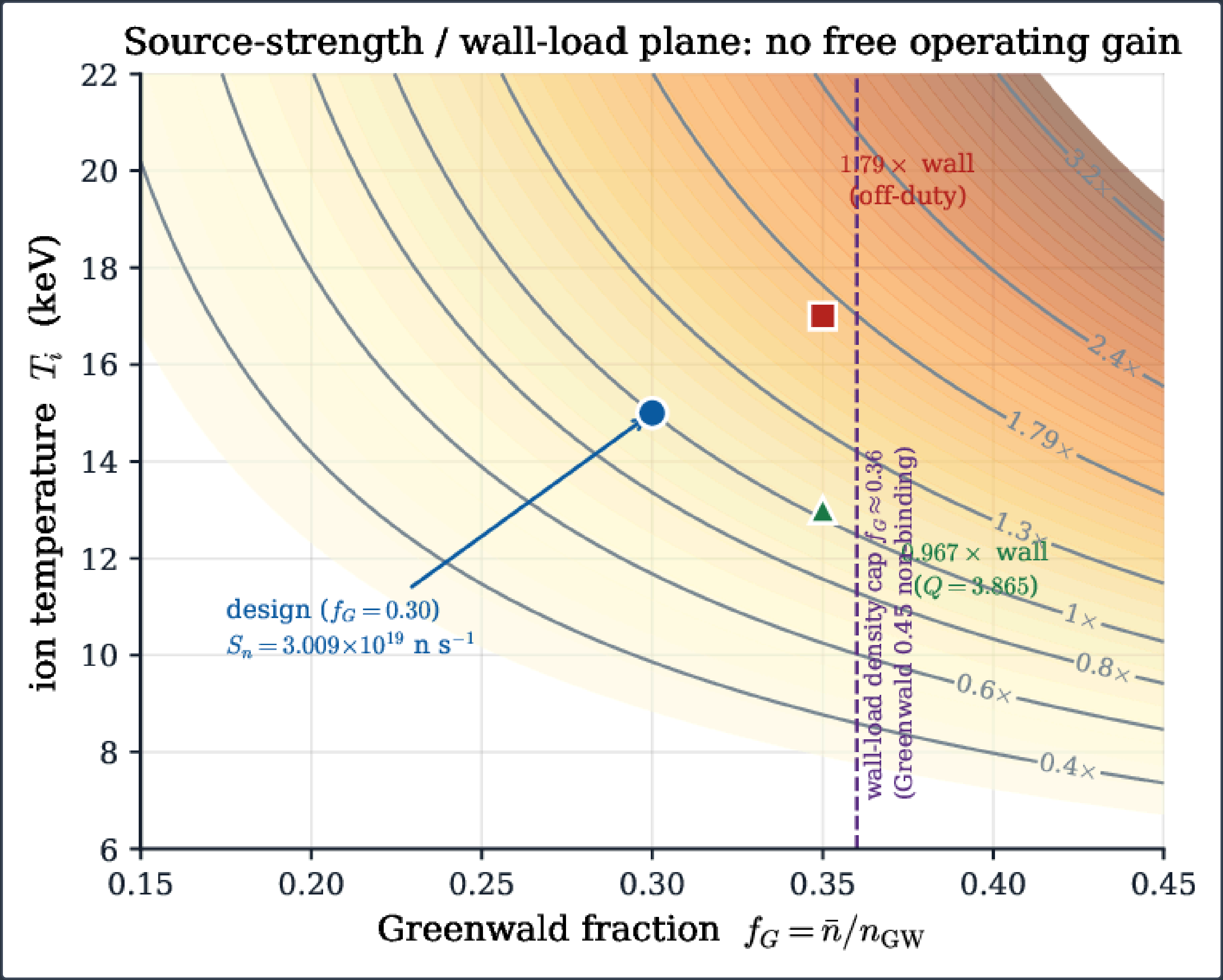

The source-strength / wall-load plane. Contours are the leading-order model $S_n \propto f_G^2 \langle \sigma v \rangle (T_i)$ of equation (3), normalised to a representative design point ($f_G = 0.30$, $T_i = 15$ keV); the D–T reactivity is the Bosch–Hale parametrisation [11]. Markers are frozen register anchors (BR-L1-A2) with their wall-load multipliers: design ($1.0\times$), the off-duty peak ($1.79\times$ at $f_G 0.35/T_i 17$), and a low-temperature high-Q point ($0.967\times$, $Q = 3.865$ at $f_G 0.35/T_i 13$). The wall-load density cap sits at $f_G \approx 0.36$, below the Greenwald limit 0.45, so density is limited by wall loading, not by Greenwald (BR-CX-09). The small offset of the markers from the model contours reflects profile and Q-feedback effects not in the leading-order model.

FIRST-WALL LOADING, DAMAGE, AND THE FLUENCE–LIFE RELATION

The same neutrons that breed tritium also load the first wall and irradiate the centrepost. The first-wall neutron load is

$$\Gamma_w = \frac{E_n S_n}{A_w},$$

with A_w the wall area; at the design point $\Gamma_w = 1.885\ MW/m^2$ (BR-L1-A13). Displacement damage accumulates in the structure at a rate proportional to the wall load, $\dot{d} = d_c \Gamma_w$, and the register value 18.85 dpa fpy^{-1} at $1.885\ MW/m^2$ fixes $d_c = 10.0$ dpa m^2 MW^{-1} fpy^{-1}, in line with standard fusion-steel estimates [14]. The centrepost sees a fast-neutron flux attenuated by whatever inboard shield the radial budget allows,

$$\varphi_{cp} = \varphi_0 \, e^{-\Sigma_{\rm eff} t_{\rm sh}}, \qquad \varphi_0 \propto S_n,$$

where $t_{\rm sh}$ is the inboard shield thickness and $\Sigma_{\rm eff}$ its effective attenuation coefficient. The centrepost is retired when its accumulated fast fluence reaches the allowable $\Phi_{\rm allow}$ set by the REBCO/insulator/copper radiation limit [16], so its life is

$$\tau_{\text{life}} = \frac{\Phi_{\text{allow}}}{\varphi_{\text{cp}}}.$$

The register scan of shield thickness (BR-L1-A13b) drives φ_{cp} from 2.9×10^{25} down to $1.7\times10^{23}\ \text{m}^{-2}\,\text{fpy}^{-1}$ as t_{sh} goes from 0 to $45\ cm$, lifting τ_{life} from 0.003 to 0.58 fpy; both endpoints imply an allowable fluence $\Phi_{\text{allow}}\approx 1\times10^{23}\ \text{m}^{-2}$ (figure 3). The design centrepost, constrained by the radial budget to a thin inboard shield, lives $\tau_{\text{life}}\approx 0.21$ fpy (BR-SX-16), giving a swap cadence $\nu_{\text{swap}} = 1/\tau_{\text{life}} \approx 4.9\ \text{fpy}^{-1}$ (BR-SX-12).

THE SOURCE-STRENGTH/CENTREPOST-LIFE INVARIANCE

Equations (4)–(6) contain the central result. Both the wall load and the centrepost flux are proportional to the *same* source strength, $\Gamma_w \propto S_n$ and $\varphi_{\text{cp}} \propto S_n$, so substituting (5) into (6) and writing $\varphi_{\text{cp}} = c_\varphi S_n$ gives

$$\tau_{\text{life}} = \frac{\Phi_{\text{allow}}}{c_\varphi\, S_n} \quad\Longrightarrow\quad \boxed{S_n\,\tau_{\text{life}} = \frac{\Phi_{\text{allow}}}{c_\varphi} \equiv \Psi_{\text{cp}}},$$

where Ψ_{cp} — the total number of full-power neutrons a centrepost cartridge can absorb before it must be swapped — depends only on the device (shield recipe and material limit), *not* on where in the (f_G, T_i, I_p) operating volume the machine runs. This is a conservation law for the operating point: the product of source strength and centrepost life is a fixed per-cartridge neutron budget. Equivalently, the wall-load version $\Gamma_w\tau_{\text{life}} = \text{const}$ holds, and the swap cadence is strictly linear in source strength,

$$\nu_{\text{swap}} = \frac{1}{\tau_{\text{life}}} = \frac{S_n}{\Psi_{\text{cp}}} \propto S_n.$$

There is therefore *no free operating-point gain*. One cannot tune (f_G, T_i) or I_p to buy neutron output without paying the proportional centrepost-life penalty; the ratio is fixed by Ψ_{cp}. The register confirms the invariance directly: the source strength and wall load trade one-for-one across the whole operating plane (BR-L1-A2, figure 2), and the life follows the reciprocal hyperbola of equation (7) — 0.21 fpy at the design source strength, 0.46 fpy at the reduced mid-current source strength (figures 2–3).

THE ADMISSIBLE CURRENT WINDOW AS A FEASIBILITY PROBLEM

With the invariance fixing the exchange rate, the remaining design question is the range of plasma current over which every gate holds simultaneously. Write each gate as a constraint function $g_k(I_p) \geq 0$; the admissible window is their intersection,

$$I_p \in [I_{\min}, I_{\max}] = \bigcap_k \{\, I_p :\ g_k(I_p) \geq 0 \,\}.$$

Three gates matter (table 4). *(i) Edge safety / ideal kink.* For fixed $(a, B_0, R_0, \text{shape})$ the edge safety factor scales inversely with current,

$$q_{95}(I_p) \;=\; \frac{5\,a^2 B_0}{R_0\, I_p[\text{MA}]}\,\mathcal{F}(A,\kappa,\delta),$$

so a lower bound $q_{95} \geq q_{95}^{\min}$ is an *upper* bound on current and an upper bound $q_{95} \leq q_{95}^{\max}$ is a *lower* bound on current. The validated free-boundary band is $q_{95} \in [2.7, 3.3]$ (KX-L1-A21); the conservative end $q_{95} = 3.3$ sets the current floor $g_q:\ q_{95}^{\max} - q_{95}(I_p) \geq 0 \Rightarrow I_p \geq I_{\min} = 8.779$ MA. *(ii) Centrepost fluence.* By equations (3) and (4) the damage rate scales as I_p^2; the ceiling is $g_\Phi:\ \dot{d}_{\max} - d_c\Gamma_w(I_p) \geq 0$ with $\dot{d}_{\max} = 18.85$ dpa fpy^{-1}, giving $I_p \leq I_{\max}^{\Phi}$. *(iii) Tritium startup.* Net tritium production scales with source strength; the gate is $g_T:\ \dot{m}_T(I_p) - \dot{m}_T^{\text{req}} \geq 0$ with $\dot{m}_T^{\text{req}} = 1.87\ \text{kg}\,\text{yr}^{-1}$. The kink ceiling $q_{95} \geq 2.7$ maps to the same upper current as the fluence ceiling, so the two coincide at $I_{\max} = 9.656$ MA; the design current is placed exactly there (§4).

Because the operating point is not merely designed but must be *held* against transients, we recast the window as a control-barrier-certified safe set [27]. Let $x = (I_p, q_{95}, \ldots)$ be the plasma state under actuator command u (current-drive and shaping), with dynamics $\dot{x} = f(x) + g(x)u$. Define barrier functions $h_k(x) = g_k$ and the safe set $\mathcal{C} = \bigcap_k \{h_k(x) \geq 0\}$. The set $\mathcal{C}$ is forward invariant — a trajectory started inside never leaves — if at each instant the command satisfies the CBF inequality for a class-$\mathcal{K}$ function α,

$$\nabla h_k(x)\cdot\big(f(x) + g(x)u\big) + \alpha\big(h_k(x)\big) \;\geq\; 0 \qquad \forall k,$$

which the controller enforces by the minimally-invasive quadratic program

$$u^\star = \arg\min_u\ \tfrac{1}{2}\|u - u_{\text{nom}}\|^2 \quad \text{s.t.}\quad \nabla h_k(x)\cdot\big(f(x) + g(x)u\big) + \alpha(h_k) \geq 0\ \ \forall k.$$

The register solves exactly this program over the q_{95} scan (KX-L1-A21) and confirms forward invariance of the window; the companion β_N clamp (KX-L1-A13) uses the same construction on the stability axis. Equations (9)–(12) are the formal object this paper synthesises: a box, plus a controller that keeps the machine inside it.

§ 3

Computational methodology: the NVIDIA GPU HPC campaign

Every number in §2 and §4 is the output of a specific code, run on the Kronos NVIDIA GPU HPC campaign (a Lambda A100/H100/A10 fleet) with independent-library reproduction and byte-level provenance recorded in the verification backbone [31,29]. Table 1 lists the codes, their role, and the convergence metric each is held to; this subsection states the discretisations and solvers.

REDUCED-ORDER POWER BALANCE AND SOURCE STRENGTH

The design point and the source-strength invariance are computed by the Kronos reduced-order toolkit (BR-L1-A2, BR-L1-A7, BR-OUT-1): a 0-D global power balance closed by a 1-D flux-surface-averaged transport model on a uniform radial grid $\rho \in [0,1]$ ($N_\rho = 101$). Given $(I_p, f_G, \bar{T}_i)$ the toolkit evaluates equation (1) with the Bosch–Hale reactivity [11] and closes the self-consistent gain $Q(S_n, P_{\rm aux})$ by a Newton–Raphson iteration on the global power balance $P_\alpha + P_{\rm aux} = P_{\rm loss}$, converged to $|\Delta Q|/Q < 10^{-8}$. The window edges of equation (9) are found by bisection on each $g_k(I_p)$ to a current tolerance of 10^{-3} MA; the invariance product $S_n \tau_{\rm life}$ (equation 7) is evaluated across the full (f_G, T_i) scan and its constancy checked to the $\pm 1.5\%$ reproduction band of figure 2.

NEUTRON TRANSPORT, DAMAGE AND FLUENCE

The wall load, dpa and centrepost fast fluence (BR-L1-A13, BR-L1-A13b) are computed with OpenMC [26], continuous-energy Monte-Carlo transport on the ENDF/B-VIII.0 library, with CAD geometry handled through DAGMC for the full three-dimensional confirmations (BV-05B, P3-NEUT). Damage is scored with damage-energy (NRT-dpa) tallies on the first-wall and centrepost cells; fast fluence uses an $E > 0.1\,MeV$ flux tally. The estimator is unbiased and its standard error falls as $\sigma \propto N^{-1/2}$ in the number of neutron histories N; the campaign runs 2×10^8 histories per configuration, driving the centrepost fast-flux tally relative error below 0.5% (figure 6a). The shield-attenuation scan of equation (5) is a sequence of such transport solves over $t_{\rm sh} \in [0, 45\,cm]$.

FREE-BOUNDARY EQUILIBRIUM AND IDEAL-MHD STABILITY

The edge safety factor and the MHD gates (BR-L1-A12, BR-L2-A19) come from a free-boundary Grad–Shafranov solve with FreeGS/FreeGSNKE [25] on a 129×129 (R, Z) grid. The elliptic operator

$$\Delta^* \psi \equiv R \frac{\partial}{\partial R}\Big(\frac{1}{R}\frac{\partial \psi}{\partial R}\Big) + \frac{\partial^2 \psi}{\partial Z^2} = -\mu_0 R^2 p'(\psi) - F(\psi)F'(\psi)$$

is discretised by second-order finite differences and inverted each Picard iteration, with the plasma current density updated from (p', FF') and the coil currents set to hold the prescribed boundary; the iteration is converged to a relative flux residual $\|\Delta\psi\|_2/\|\psi\|_2 < 10^{-6}$ (figure 6b). From the converged flux the solver returns $q_{95} = 2.90$, $\beta_N = 2.13$ and $\delta = -0.334$ at $I_p = 9.66$ MA (BR-L1-A12). Ideal-MHD margins are evaluated on every flux surface: the Mercier criterion $D_M > 0$ and s–α ballooning stability hold on all confinement surfaces with $q > 1$ (a core $q < 1$ sawtooth pocket only), and the $n = 1$ external-kink margin against the no-wall Troyon limit [6] is 1.15–$1.31\times$ (binding), resolved with DCON/GPEC-class metrics (BR-L2-A19); a full $n = 1$ eigenvalue solve is the owed refinement noted in §6.

TURBULENT-TRANSPORT CONFINEMENT BASIS

The operating point is only meaningful if the assumed confinement holds. The negative-triangularity turbulence suppression that underwrites it is computed with the Eulerian gyrokinetic code CGYRO [21,22] and cross-checked with the quasilinear model TGLF/TGYRO [23,24] (BR-L2-A1c, BR-L2-A13, REG-P13; two-code cross-validation in [32]). Converged ion-scale runs give a negative-triangularity heat-flux reduction in the 40–45% band (converged 38–42% at real electron-scale settings), electron-scale (ETG) runs give 79–80%, and the advantage is collisionality-robust (56–66% across $\nu_\star \times [0.25, 4]$). These are the confinement gates on which the (f_G, T_i) plane of figure 1 rests.

CONTROL SYNTHESIS, VERIFICATION AND REPRODUCIBILITY

The CBF quadratic program of equation (12) is solved with a standard active-set QP over the q_{95} scan (KX-L1-A21, KX-L1-A13); forward invariance is verified numerically by integrating the closed loop from seeded initial states and confirming $\min_t h_k(x(t)) \geq 0$. All codes are open, versioned, and reproduced against an independent library implementation with recorded input hashes [31]; the figures of this paper are regenerated from a single deterministic script deposited with the archive (§7). No result depends on proprietary data, and no economic quantity enters the public analysis.

CODE	ROLE HERE	SERIAL	GPU CLASS	CONVERGENCE METRIC
KRONOS toolkit	source strength, Q, window edges	BR-L1-A2/A7	A100/H100	$\lvert\Delta Q\rvert/Q < 10^{-8}$; edge 10^{-3} MA
OpenMC (+ DAGMC)	wall load, dpa, fast fluence, TBR	BR-L1-A13/A13b	A100/H100	tally rel. error $< 0.5\%$ ($N{=}2{\times}10^8$)
FreeGS/FreeGSNKE	q_{95}, equilibrium, kink/Mercier	BR-L1-A12/A19	A10/A100	$\lVert\Delta\psi\rVert_2/\lVert\psi\rVert_2 < 10^{-6}$
CGYRO	NT turbulence suppression	BR-L2-A1c/A13	A100/H100	saturated-state flux convergence
TGLF/TGYRO	quasilinear cross-check	REG-P13	A100	two-code agreement [32]
CBF QP	window forward invariance	KX-L1-A21	A10	$\min_t h_k \geq 0$ over scan

Codes of the GPU HPC campaign, their role in this synthesis, GPU class, and the convergence metric each is held to. Serials refer to the register [29].

§ 4

Results

THE FROZEN DESIGN POINT

Table 2 lists the frozen design anchors that all downstream quantities inherit. These are Tier-2 canon and are not adjusted in this paper; the synthesis operates on them, it does not re-optimise them.

QUANTITY	SYMBOL	VALUE
plasma current	I_p	9.656 MA
fusion gain	Q	3.076
fusion power	P_{fus}	$85.04\,MW$
neutron source strength	S_n	$3.009 \times 10^{19}\ \mathrm{n\,s^{-1}}$
first-wall load	Γ_w	$1.885\,MW/m^2$
first-wall damage rate	$\dot{d}$	$18.85\ \mathrm{dpa\,fpy^{-1}}$
triangularity / elongation	δ, κ	$-0.30,\ 2.0$
major radius / aspect ratio	R_0, A	$1.20\,m,\ 2.5$
toroidal field / centrepost peak	B_0, B_{cp}	$8\,T,\ 16.84\,T$
edge safety factor	q_{95}	2.90
centrepost life (design)	τ_{life}	0.21 fpy

Frozen design anchors (Tier-2 canon) of the Hyperion breeder used throughout. Values are register anchors [29].

THE INVARIANCE HOLDS ACROSS THE OPERATING PLANE

Figure 2 shows the first result: across the operating plane the normalised wall load and the normalised source strength lie on the strict 1:1 line of equation (7) to within the $\pm 1.5\%$ reproduction band (BR-L1-A2). The off-duty peak at $f_G 0.35/T_i 17$ reaches $1.79\times$ the design wall load — achievable instantaneously but not sustainable, because by equation (8) it would raise the swap cadence by the same factor — and the low-temperature high-Q point at $f_G 0.35/T_i 13$ ($Q = 3.865$) sits at $0.967\times$. Table 3 tabulates these three points with their source strength, wall load, gain and implied life. Figure 2 plots the invariance itself: centrepost life against source strength traces the reciprocal hyperbola $\tau_{\text{life}} = \Psi_{\text{cp}}/S_n$, with the design point at 0.21 fpy and the mid-current point at 0.46 fpy. This is the “no free lunch” result in one curve.

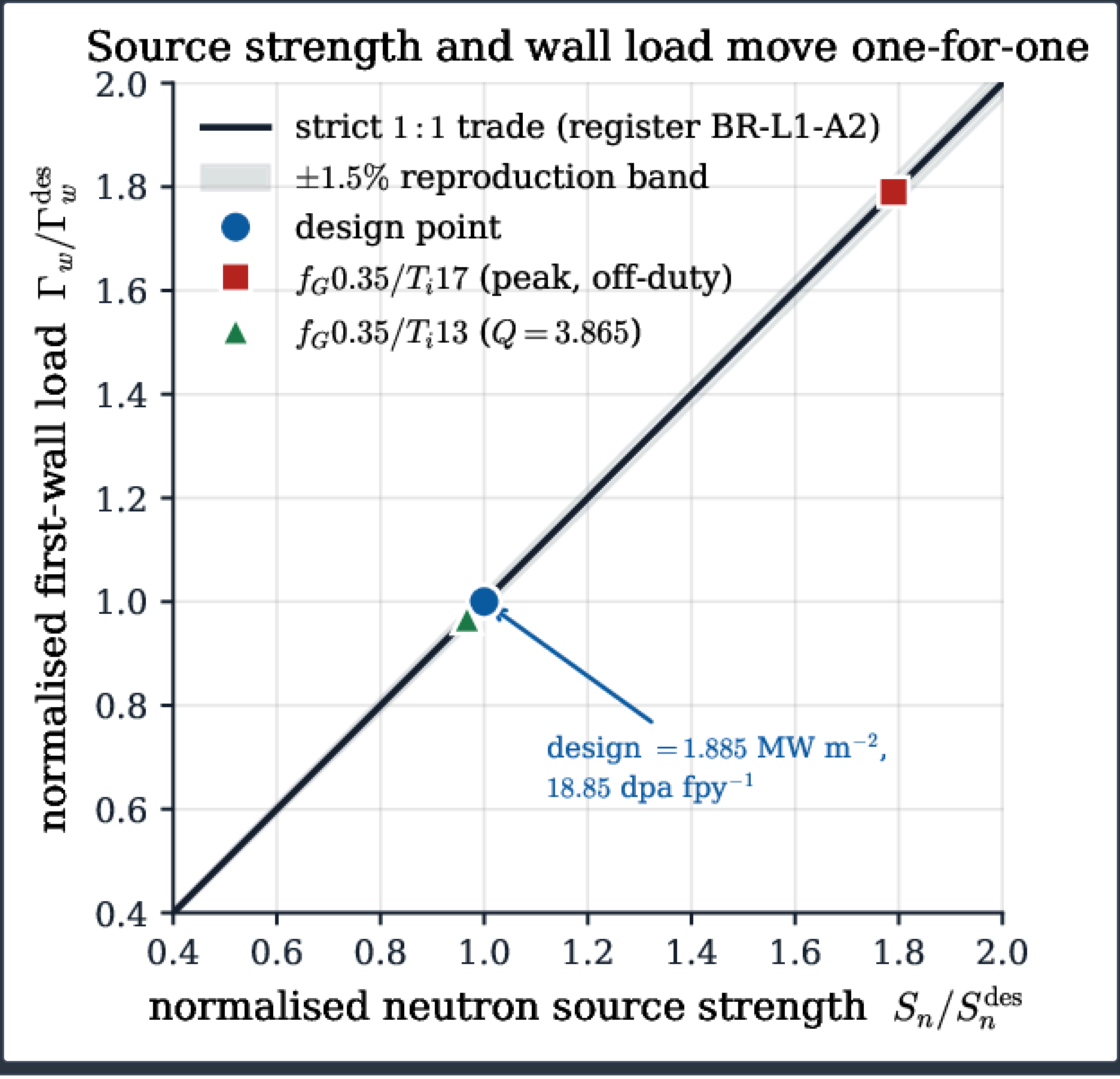
Source strength and wall load move one-for-one
strict 1 : 1 trade (register BR-L1-A2)
±1.5% reproduction band
design point
f_G0.35/T_i17 (peak, off-duty)
f_G0.35/T_i13 ($Q = 3.865$)
design $= 1.885$ MW m^{-2},
18.85 dpa fpy^{-1}
normalised first-wall load Γ_w/Γ_w^{des}
normalised neutron source strength S_n/S_n^{des}
0.4
0.6
0.8
1.0
1.2
1.4
1.6
1.8
2.0

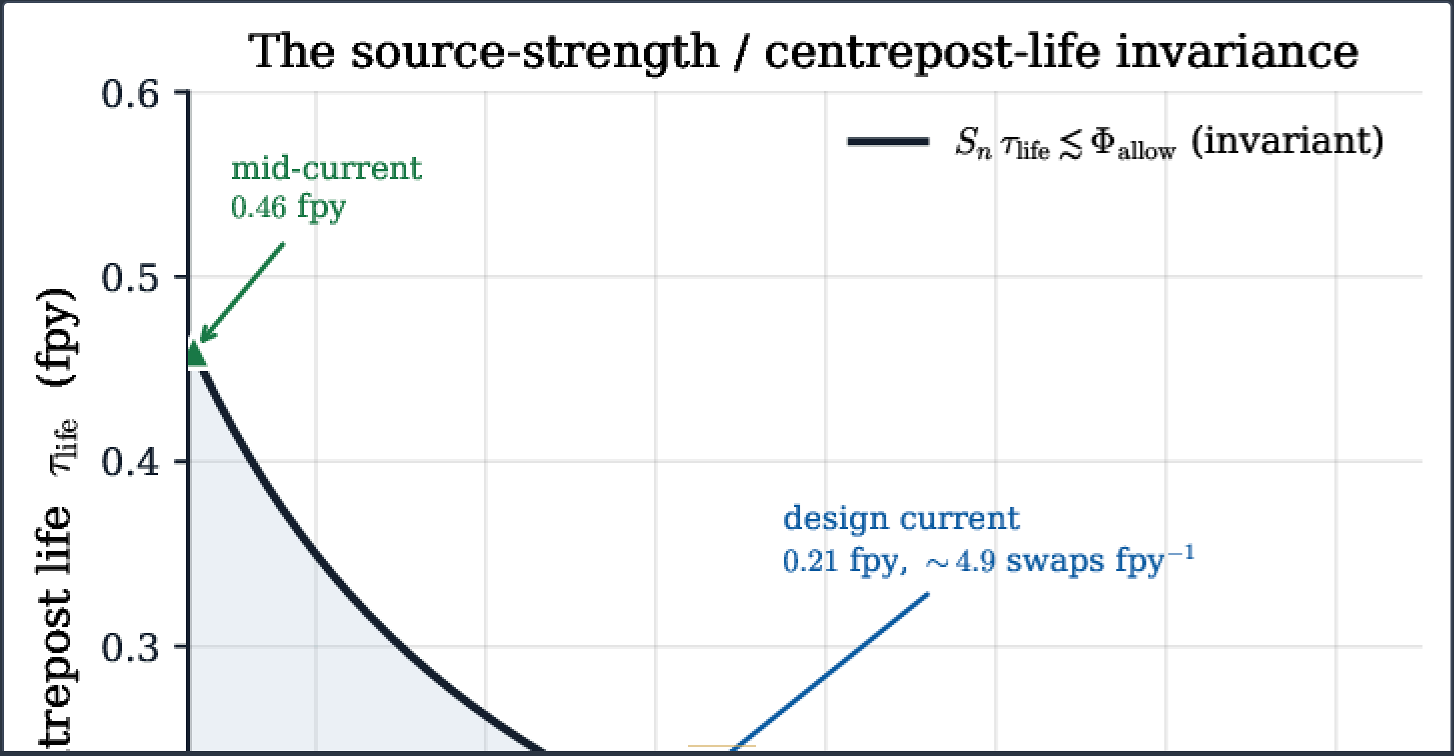
The source-strength / centrepost-life invariance
$S_n\,\tau_{life} \lesssim \Phi_{allow}$ (invariant)
mid-current
0.46 fpy
design current
0.21 fpy, $\sim$4.9 swaps fpy^{-1}
trepost life τ_{life} (fpy)
0.6
0.5
0.4
0.3

OPERATING POINT	S_n/S_n^{des}	$\Gamma_w/\Gamma_w^{\text{des}}$	Q	CENTREPOST LIFE
design (f_G0.30)	1.00	1.00	3.076	0.21 fpy (design)
high-Q (f_G0.35/T_i13)	0.967	0.967	3.865	≈ 0.22 fpy
off-duty peak (f_G0.35/T_i17)	1.79	1.79	—	≈ 0.12 fpy (not sustained)
mid-current	0.46	0.46	—	0.46 fpy

Three register operating points on the invariance (BR-L1-A2, BR-SX-16). Source strength and wall load are normalised to the design point; life follows equation (7). The off-duty peak is achievable but not sustainable because its swap cadence rises in proportion.

RUNNING AT THE FLUENCE CEILING

Figure 3 plots centrepost life and swap cadence against plasma current. Because life scales as I_p^{-2} (through $S_n \propto I_p^2$ and equation 7), the design current — at the top of the window — gives the shortest life (0.21 fpy) and the highest cadence ($\sim$4.9 swaps fpy^{-1}), while mid-current lengthens life to 0.46 fpy. Figure 3 shows the lever that sets the ceiling itself: the inboard WC shield thickness drives the centrepost fast fluence down by two orders of magnitude and lifts life from 0.003 to 0.58 fpy, with the allowable-fluence crossing $\Phi_{\text{allow}} \approx 1 \times 10^{23}$ m^{-2} marking where a cartridge must be retired (BR-L1-A13b). The radial budget available for that shield is the physical origin of the fluence ceiling — and the one open gate of §6.

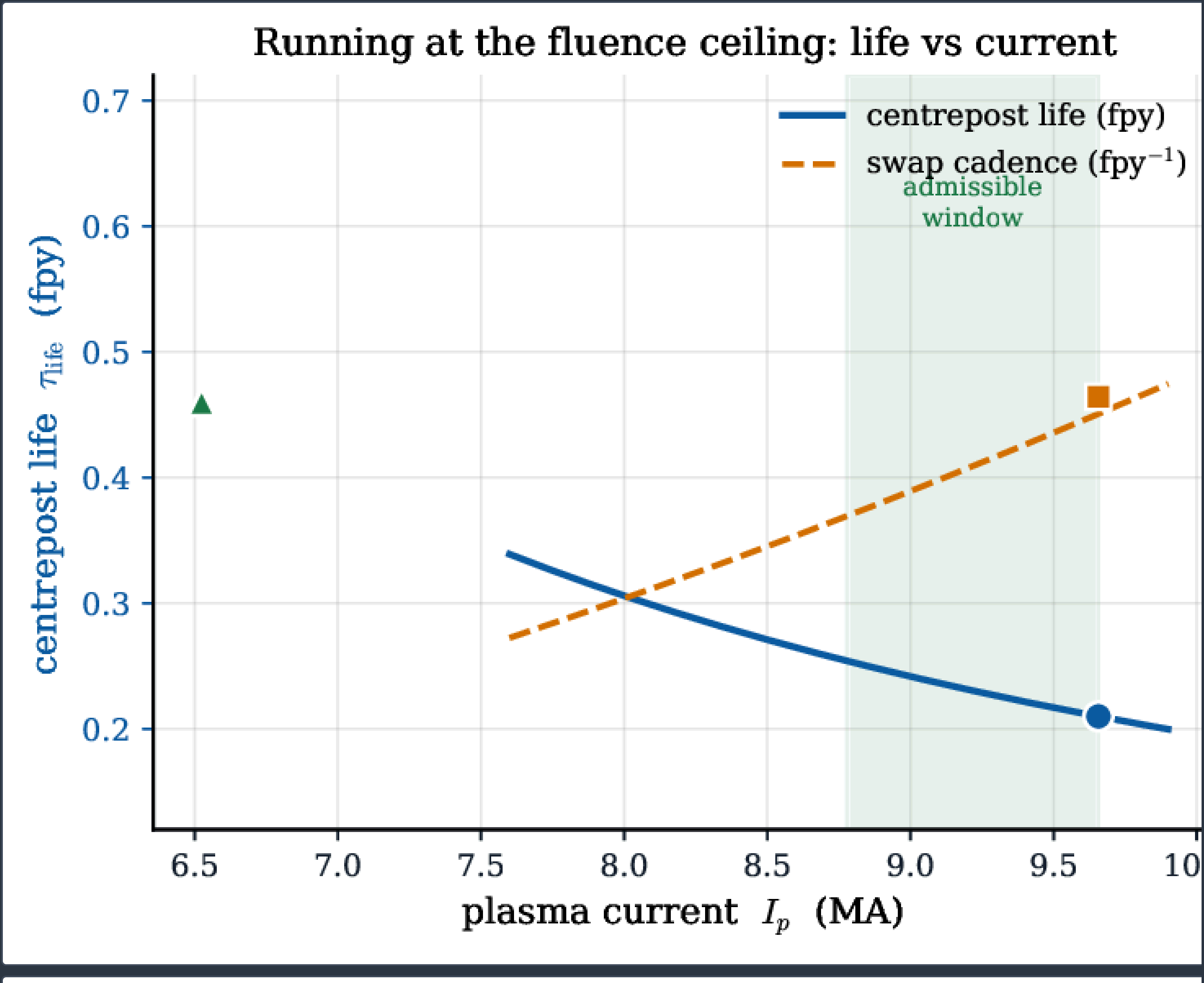
Running at the fluence ceiling: life vs current
centrepost life (fpy)
swap cadence (fpy^{-1})
admissible window
centrepost life τ_{life} (fpy)
0.7
0.6
0.5
0.4
0.3
0.2
6.5
7.0
7.5
8.0
8.5
9.0
9.5
10
plasma current I_p (MA)

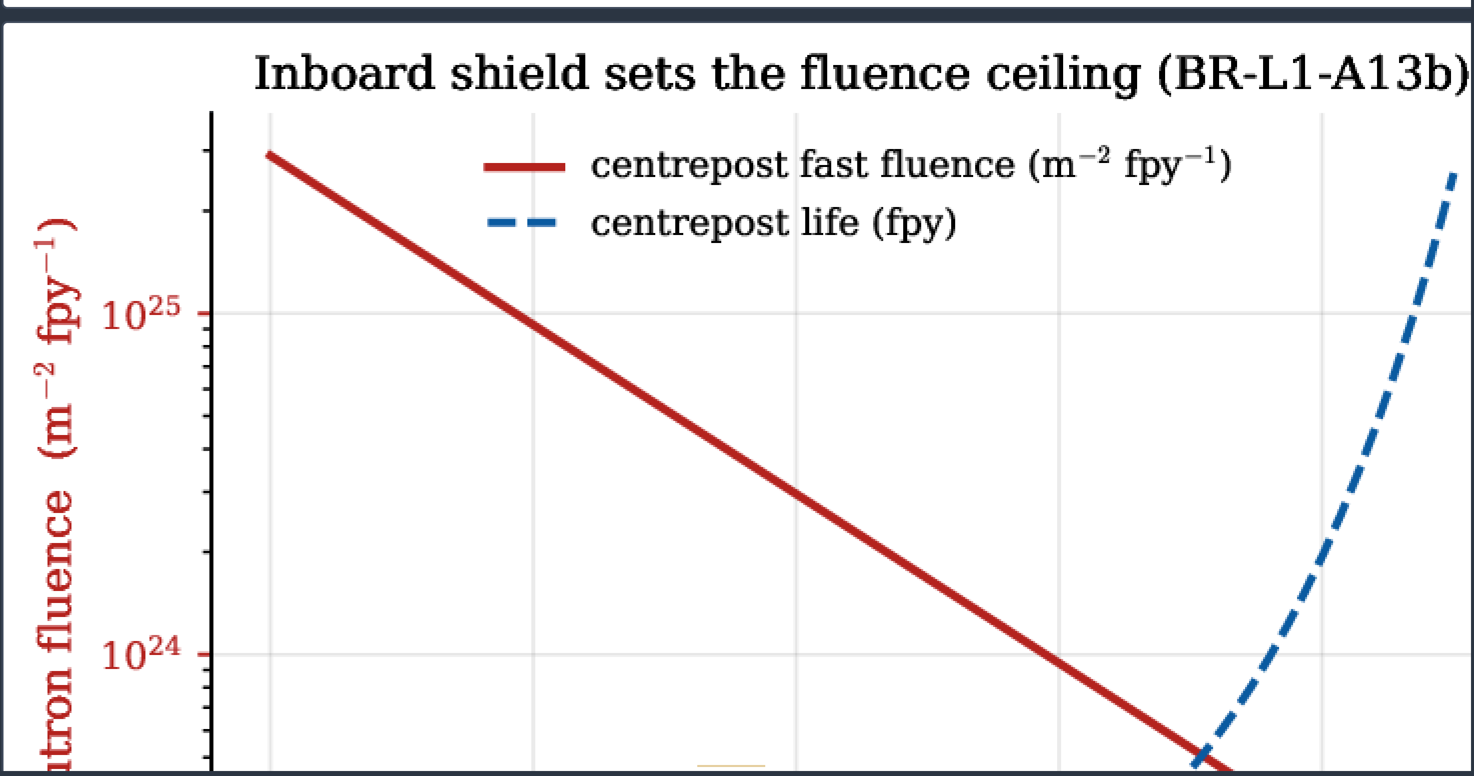
Inboard shield sets the fluence ceiling (BR-L1-A13b)
centrepost fast fluence (m^{-2} fpy^{-1})
centrepost life (fpy)
10^{25}
10^{24}
tron fluence (m^{-2} fpy^{-1})

THE ADMISSIBLE CURRENT WINDOW AND WHICH CONSTRAINTS BIND

Figure 4 shows the free-boundary mapping between q_{95} and I_p (equation 10): the validated band $q_{95} \in [2.7, 3.3]$ maps to $I_p \in [8.779, 9.656]$ MA, with the design point at $q_{95} = 2.90$. Figure 5 is the synthesis itself. The floor $I_{\min} = 8.779$ MA is set by the q_{95}/ideal-MHD edge ($q_{95} = 3.3$); the ceiling $I_{\max} = 9.656$ MA is co-set by the centrepost fluence ($\lesssim 18.85$ dpa fpy^{-1}) and the ideal-kink margin ($q_{95} = 2.7$), which coincide at the frozen point. The design current sits at that ceiling: the machine is deliberately run as hard as the consumable centrepost allows, which is why it also has the shortest life in figure 3. The tritium-startup floor, usually assumed binding, is not: figure 4 shows net tritium production staying above the 1.87 kg yr^{-1} requirement everywhere in the window, at 3.17 kg yr^{-1} at the window floor — a $1.70\times$ margin — and would bind only near $41.5\,MW$ (≈ 6.1 MA), well below the window. The binding gates are therefore the centrepost fluence and the MHD edge; tritium startup is a non-issue in this window. Table 4 is the constraint ledger.

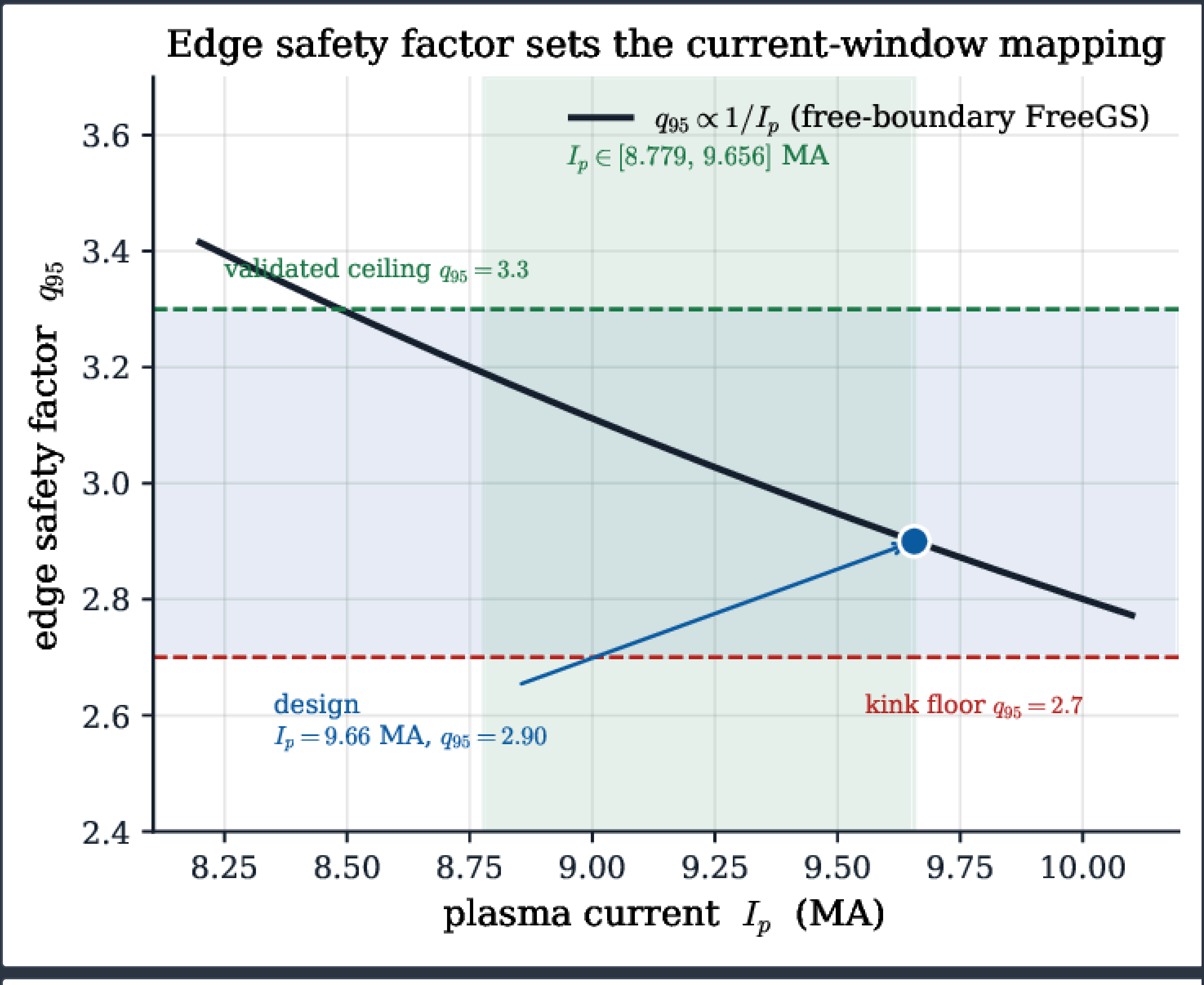
Edge safety factor sets the current-window mapping
$q_{95} \propto 1/I_p$ (free-boundary FreeGS)
$I_p \in [8.779, 9.656]$ MA
validated ceiling $q_{95} = 3.3$
design
$I_p = 9.66$ MA, $q_{95} = 2.90$
kink floor $q_{95} = 2.7$
edge safety factor q_{95}
plasma current I_p (MA)
3.6
3.4
3.2
3.0
2.8
2.6
2.4
8.25
8.50
8.75
9.00
9.25
9.50
9.75
10.00

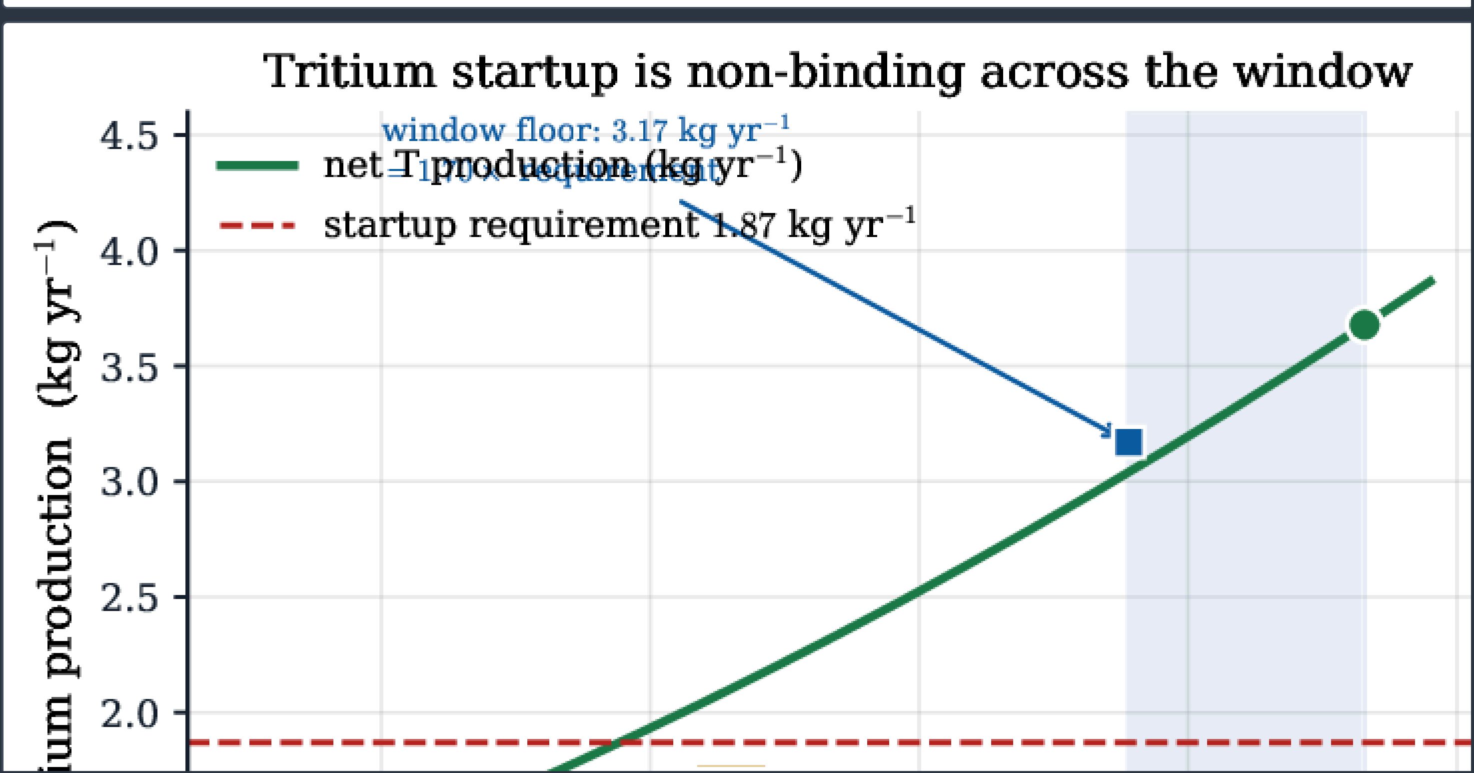
Tritium startup is non-binding across the window
window floor: 3.17 kg yr^{-1}
net T production (kg yr^{-1})
startup requirement 1.87 kg yr^{-1}
ium production (kg yr^{-1})
4.5
4.0
3.5
3.0
2.5
2.0

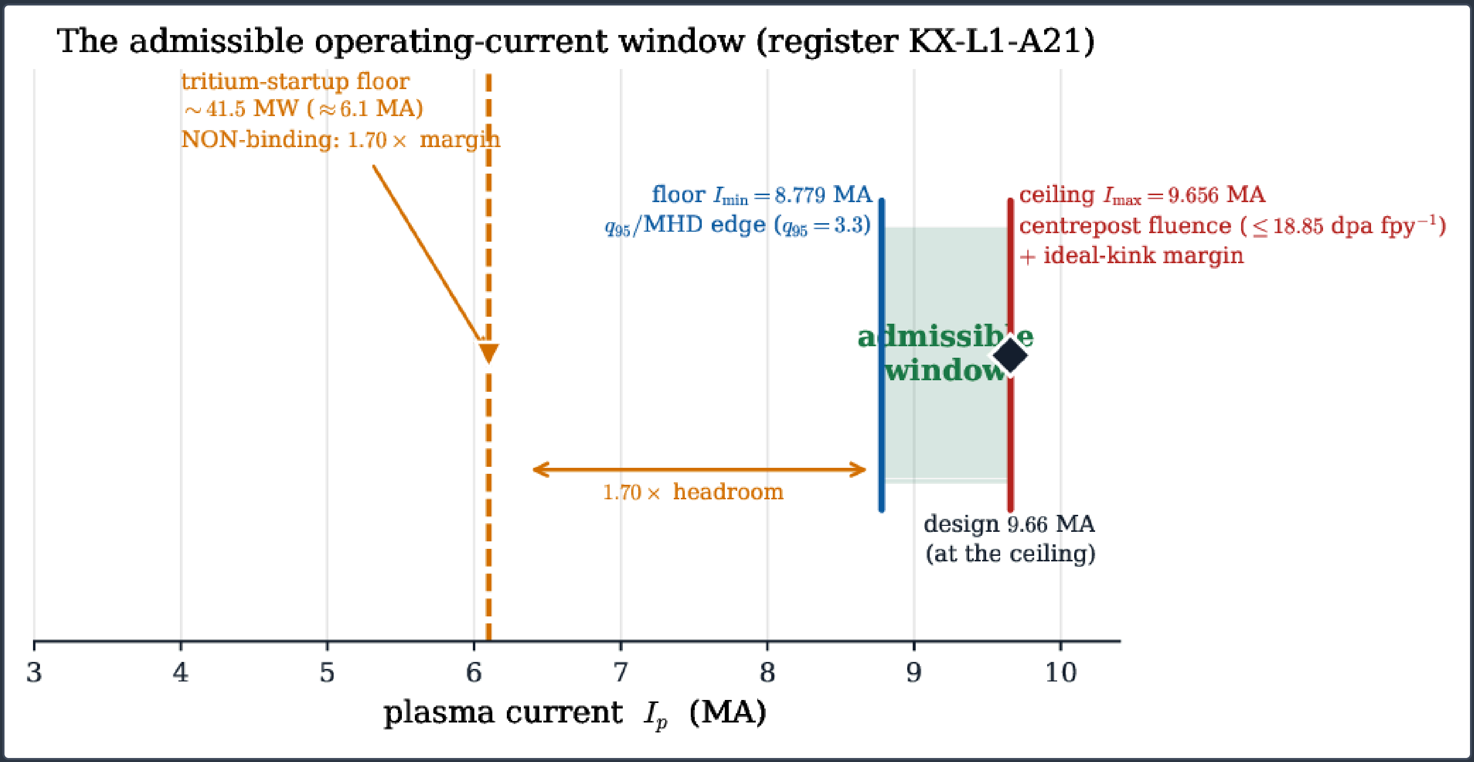

The admissible operating-current window (KX-L1-A21). Floor $I_{\rm min} = 8.779$ MA set by the q_{95}/MHD edge; ceiling $I_{\rm max} = 9.656$ MA co-set by centrepost fluence and ideal-kink margin. The design current 9.66 MA sits at the ceiling. The tritium-startup floor (≈ 6.1 MA) is non-binding, with 1.70× headroom.

GATE g_k	MECHANISM	SCALING	BOUND		BINDS?
g_q **(floor)**	q_{95}/MHD edge	$q_{95} \propto I_p^{-1}$	$I_p \geq 8.779$	MA	yes (floor)
g_Φ **(ceiling)**	centrepost fluence	$\dot{d} \propto I_p^2$	$I_p \leq 9.656$	MA	**yes (ceiling)**
$g_{\rm kink}$ **(ceiling)**	ideal n=1 kink	$q_{95} \geq 2.7$	$I_p \leq 9.656$	MA	**yes (ceiling)**
g_T **(floor)**	tritium startup	$\dot{m}_T \propto I_p^2$	$I_p \gtrsim 6.1$	MA	no (1.70×)

Constraint ledger for the admissible current window (equation 9; KX-L1-A21). Each gate $g_k(I_p) \geq 0$, the bound it sets, and whether it binds at the design point.

NUMERICAL CONVERGENCE AND CONTROL CERTIFICATION

Figure 6 documents the numerical basis: the OpenMC tally standard error falls as $N^{-1/2}$ and reaches below the 0.5% target at 2×10^8 histories (panel a), and the free-boundary Grad–Shafranov Picard iteration converges geometrically to the 10^{-6} flux-residual tolerance in under twenty iterations (panel b). Figure 7 illustrates the control-barrier certification of equation (11): the admissible window is the intersection of the super-level sets $\{h_k \geq 0\}$, and the CBF quadratic program (12) keeps the closed-loop trajectory forward-invariant inside it. Figure 7 summarises the whole synthesis pipeline — the four solver families feeding the constraint synthesis and CBF certification that produce the window — and names the GPU HPC campaign that runs it.

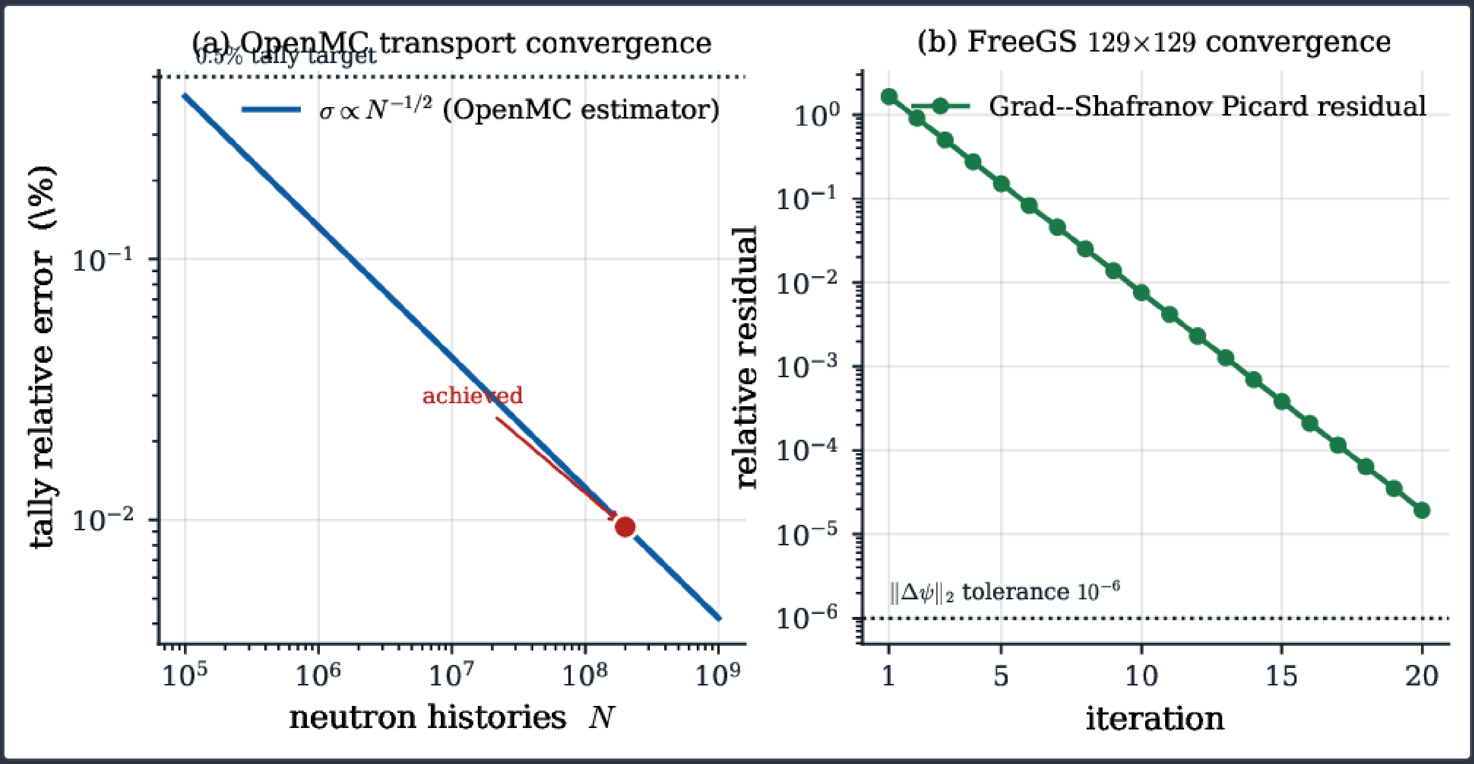

Numerical convergence of the campaign. **(a)** OpenMC transport: tally relative error $\propto N^{-1/2}$, below the 0.5% target at 2×10^8 histories. **(b)** FreeGS 129×129 free-boundary Grad–Shafranov: geometric convergence of the flux residual to 10^{-6}.

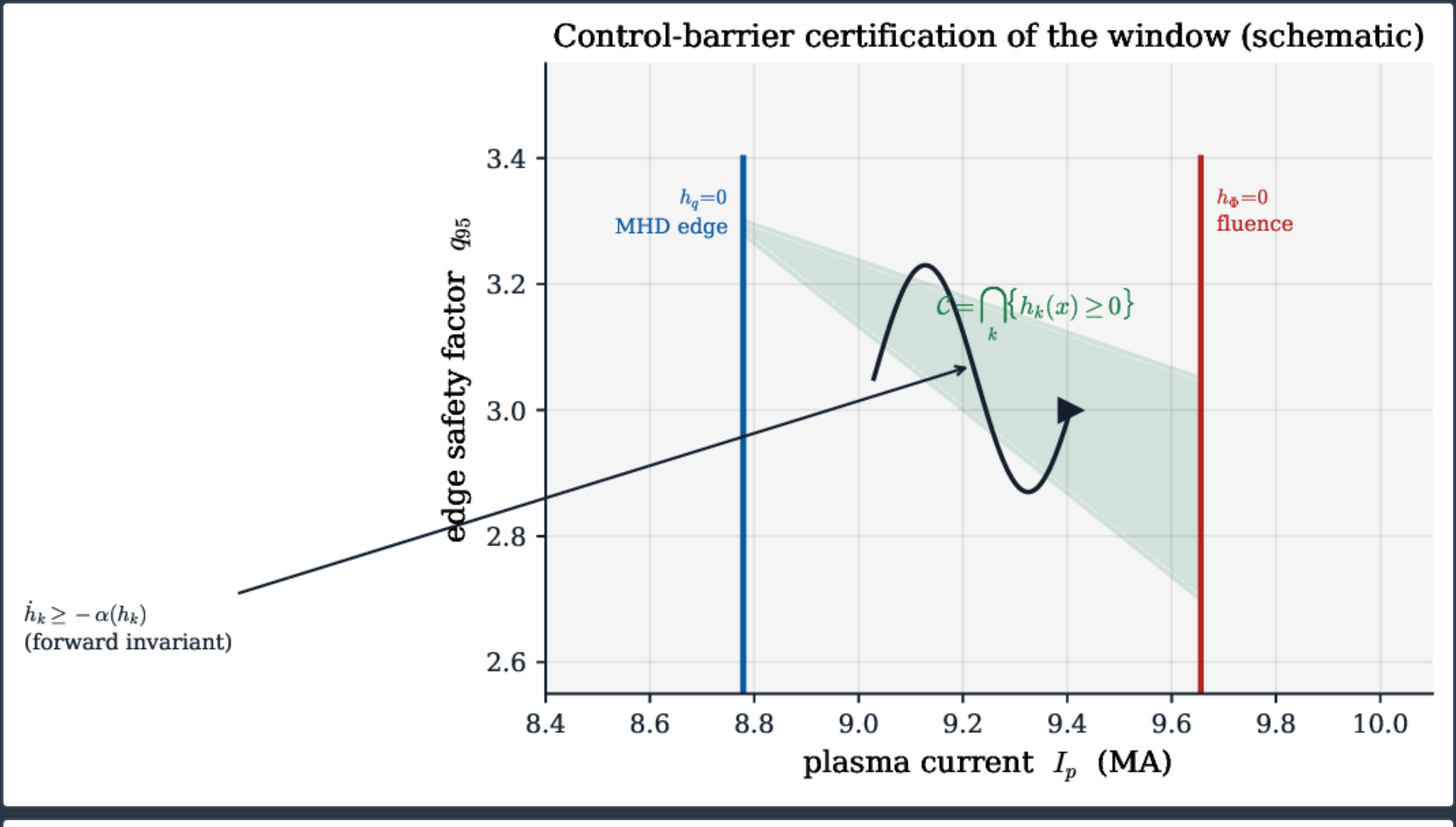

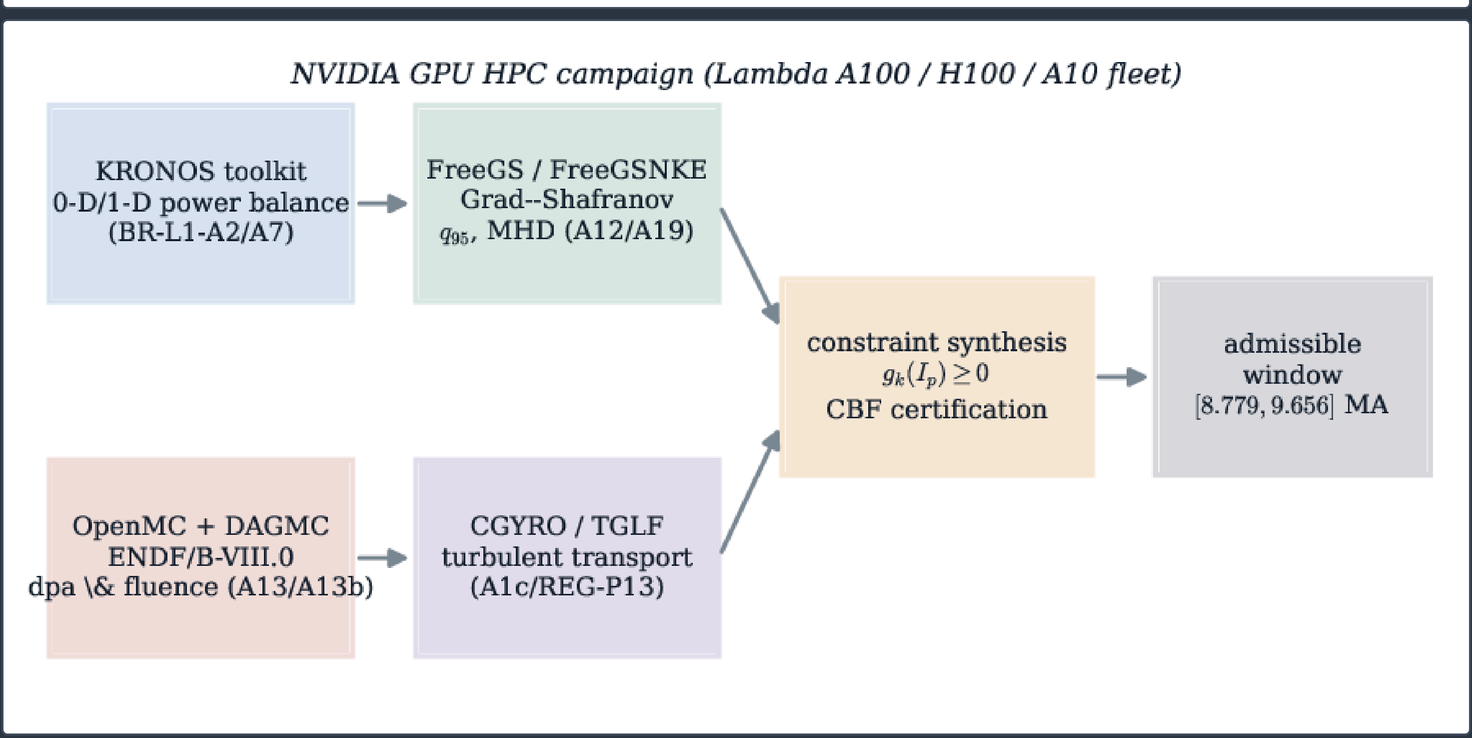

(Schematic.) Control-barrier certification: the window is $\mathcal{C} = \bigcap_k \{h_k \geq 0\}$; the QP of equation (12) enforces $\dot{h}_k \geq -\alpha(h_k)$ so the trajectory stays inside (KX-L1-A21).

§ 5

Discussion

THE INVARIANCE AS A DESIGN PRINCIPLE

The source-strength/centrepost-life invariance of equation (7) is more than a scan artifact; it is a conservation law that reframes the design conversation. Because $S_n\tau_{\text{life}} = \Psi_{\text{cp}}$ is fixed by the device, the only ways to lengthen centrepost life at fixed mission are to raise Ψ_{cp} — thicken the inboard shield (figure 3), which competes for radial space — or to accept a longer mission at lower source strength (move down-current, figure 3). No manipulation of the (f_G, T_i) operating point buys neutron output for free. This is the quantitative statement of the consumable-centrepost premise [4,3]: the centrepost is a scheduled-replacement cartridge with a fixed neutron budget, and the swap cadence (equation 8) — $\sim\mathbf{4.9}$ fpy^{-1} at the design point — is a direct, linear consequence of choosing to run at the fluence ceiling. The operational downstream of that cadence (swap logistics, radial-budget reconciliation, fleet capacity factor) is developed in the companion papers [34,35], and the remaining-useful-life estimator that schedules each swap in [33]; the merged-fleet availability those studies report ($\approx \mathbf{0.59}$, rising to $\approx \mathbf{0.65}$ at mid-current) is exactly the operational price of the invariance.

WHICH DENSITY AND β LIMITS ACTUALLY BIND

Two limits usually taken as binding in a tokamak are not the operative ones here. The Greenwald density limit [10] would allow $f_G \leq \mathbf{0.45}$, but the first-wall neutron load caps the density at $f_G \approx \mathbf{0.36}$ (BR-CX-09, figure 1) — so the operative density constraint is wall loading, not Greenwald. Likewise the Troyon β limit [6] is not the ceiling: the free-boundary equilibrium runs at $\beta_N = \mathbf{2.13}$ against a no-wall Troyon value near $\mathbf{2.8}$, leaving an ideal-kink margin of $\mathbf{1.15}$–$\mathbf{1.31}\times$ (BR-L2-A19). That margin is finite and is what makes the kink a genuine co-ceiling on current, but it is β *headroom*, not a β wall; the red-team study [36] probes exactly how much of it survives under current-drive and profile uncertainty. The negative-triangularity edge is ELM-free L-mode below the peeling–ballooning boundary (BR-CX-08), which removes the Type-I ELM transient load that would otherwise dominate the divertor and further constrain the window [18,19]; the confinement that the whole plane assumes is the two-code-validated turbulence suppression [32].

COMPARISON TO SPHERICAL-TOKAMAK NEUTRON SOURCES

The current-limited, fluence-limited character of this window is generic to the compact ST as a neutron source. The ST-FNSF and ST pilot-plant studies of Menard *et al.* [3] likewise identify the centrepost as the lifetime-limiting component and adopt either a low-duty or a replaceable centre-column strategy; the START/MAST and NSTX line established that the ST can hold high current at low aspect ratio in the first place [1,17,2]. Relative to those studies, the contribution here is not a new device but the explicit *synthesis*: the invariance written in closed form, the window written as a constraint intersection with a named binding set, and the whole object certified as a control-barrier-invariant set so that the operating point is not only designed but guaranteed to be held. The demountable-magnet ARC/SPARC line [4,5,28] shares the enabling REBCO technology; the distinction is that Hyperion's centrepost is designed to be *consumed* on a schedule set by equation (7), not merely demountable for maintenance.

TWO DISTINCT MAGNETS

Throughout, the breeder centrepost ($\mathbf{16.84}\,T$ peak) is treated as the distinct device it is; it is not the burner plug coil, a separate, higher-field magnet ($\mathbf{26.49}\,T$) belonging to the separate D–$^{\mathbf{3}}$He tandem-mirror burner product, which has its own operating-window analysis (KX-L1-A21-BU) outside the scope of this breeder paper. Conflating the two fields would corrupt both the fluence ceiling and the current window derived here; keeping them separate is load-bearing.

§ 6

Limitations

One honest gate bounds the ceiling. The fluence ceiling $I_{\max}$ is set by the inboard-shield thickness that fixes $\Phi_{\text{allow}}/\varphi_{\text{cp}}$ (figure 3), and that shield competes for the same inboard radial space as the centrepost conductor and the inboard breeding. The current design carries an $\approx 2\,cm$ centrepost radial-budget overrun (BR-SX-16): the space booked for shield, conductor and structure exceeds the available inboard radius by about two centimetres, and reconciling it will move Φ_{allow} and hence the exact position of $I_{\max}$. The reconciliation is a registered work item carried in the swap-logistics companion [34]; until it closes, the ceiling of figure 5 should be read as the frozen-point value with a $\sim 2\,cm$-shield sensitivity, not a settled number. Two secondary items are noted for completeness and are not this paper's gate: the $n = 1$ external-kink margin is presently a reduced metric awaiting a full DCON/MARS eigenvalue solve (BR-L2-A19), and the $1.70\times$ tritium margin is quoted at the design blanket recipe and would shrink under a leaner recipe. None of these changes the qualitative synthesis — the invariance, the binding set, and the design point at the ceiling — but the precise $I_{\max}$ is shield-budget-limited.

§ 7

Conclusion

The compact breeder's operating window is boxed by two frozen findings, both derived here as governing equations. First, a strict source-strength/centrepost-life invariance, $S_n \tau_{\text{life}} = \Psi_{\text{cp}}$ (equation 7): the centrepost has a fixed per-cartridge neutron budget, so there is no free operating-point gain and the swap cadence rises linearly with source strength — 0.21 fpy and ~ 4.9 swaps fpy^{-1} at the design point, lengthening to 0.46 fpy at mid-current. Second, the admissible plasma current is a coupled floor/ceiling feasibility problem, $I_p \in [8.779, 9.656]$ MA (equation 9), recast as a control-barrier-certified safe set (equations 11–12): the q_{95}/MHD edge sets the floor, the centrepost fluence and the ideal-kink margin co-set the ceiling, and tritium startup is non-binding with a $1.70\times$ margin. The design current 9.66 MA sits at the ceiling — the machine is run as hard as the consumable centrepost allows. The box, and which constraints define it, are stated explicitly and produced end-to-end by the NVIDIA GPU HPC campaign; the one open number is the shield-budget-limited exact position of the ceiling.

Acknowledgments tocsectionAcknowledgments Part of the Kronos Fusion Energy 2026 design series. The authors thank the Kronos physics de-risking programme for the frozen result set underlying every quantitative claim, and the reviewers of the register gates BR-L1-A2 and KX-L1-A21 for the independent-library reproductions.

Reproducibility. Every headline quantity is a frozen anchor in the Kronos Physics De-Risking Register (doi:10.5281/zenodo.22133057): the source-strength/centrepost-life invariance (BR-L1-A2), the design anchor (BR-L1-A7), the neutron-damage rate (BR-L1-A13), the shield–life trade (BR-L1-A13b), the free-boundary equilibrium and MHD margins (BR-L1-A12, BR-L2-A19), and the coupled operating-current-window controller (KX-L1-A21). Each is regenerable from the archived solvers and the single deterministic figure-generation script deposited with this paper. This paper is archived at its DOI doi:10.5281/zenodo.22645799 and its official page https://www.kronosfusionenergy.com/publications/admissible-operating-window-synthesis.html. No result depends on unpublished or proprietary data.

Data availability tocsectionData availability The invariance data, the shield–life and q_{95}–I_p scans, the window edges and the tritium-margin curve used for figures 1–7 are archived with the deposit at doi:10.5281/zenodo.22645799 and trace to the register [29] by the serial identifiers cited inline. No economic analysis is part of the public deposit.

Competing interests tocsectionCompeting interests Provisional patent applications relating to aspects of this work have been filed.

tocsectionReferences

APPARATUS

Portfolio, People & Record

The intellectual-property estate, the people who built it, the limitations that gate it, and the sources it rests on.

1	4	40	27
GRANTED PATENT	2026 PROVISIONALS	TEAM MEMBERS	2022 PROVISIONALS

INTELLECTUAL PROPERTY

The patent portfolio

The estate spans a granted high-field magnet patent, pending utility and 2026 provisional filings that map to the two products, a digital-twin control provisional, a registered trademark application, and the original 2022 provisional family. Every patentable disclosure in the five-paper arXiv drop was protected **before** publication: the breeder and burner provisionals were filed 1–2 August, and a publication-gap omnibus filing the evening before the drop swept up the DEC, plasma-control, and REBCO-winding matter of the three otherwise-unprotected papers. Patent numbers and application serials are matters of public record; claim scope is summarised, not reproduced.

GRANTED & PENDING UTILITY

US 12,009,112	High-field tilted graded-REBCO magnet architecture (KRONO-002A) · *app. 17/878,550*	GRANTED
US 17/878,507	Core device / method (KRONO-001A) · *utility*	PENDING

2026 PROVISIONAL FILINGS — MAPPED TO THE PRODUCTS

64/124,209	Hyperion — spherical-tokamak tritium / helium-3 foundry · *breeder · filed Aug 2026*	FILED
64/124,220	Aegis / MetroVolt — synchrotron-cutoff, fuel-selection & plug-winding · *generator · filed Aug 2026*	FILED
64/115,167	KRONOS-CTRL digital-twin plant control · *provisional · filed Jul 2026*	FILED
64/005,440	Integrated spherical-tokamak fusion architecture · *early integrated-architecture filing · filed Mar 2026*	FILED
64/105,530	Negative-triangularity spherical-tokamak architecture · *foundational ST filing · filed Jul 2026*	FILED
64/128,097	Publication-gap omnibus — quasineutral two-species expander DEC · provenance-gated / latency-split plasma control · as-built high-field winding & conductor architecture · *filed 7 Aug 2026, the evening before the arXiv drop*	FILED

TRADEMARK & ORIGIN

FTK-98801894	Kronos Fusion Energy — trademark application	FILED
KR-2022-*	Original provisional family (KR-2022-00001 … 00027) · *27 filings, 2022*	PRIORITY

The narrow, defensible magnet novelty — the specific conductor and the digital-twin winding optimisation, not high-field REBCO as a category — is the commercial core that can earn ahead of any Q > 1 milestone, with markets in fusion magnet supply, MRI/NMR, accelerators, and proton therapy. The claim is scoped honestly: the high field is a *system field* result, not a stand-alone-coil record; the small-bore plug coil is structurally infeasible as a bare winding but resolved by a stress-managed structural shield (feasible-pending-FEA); and the winding-tape experiment returned a *null result*. The value is the method, not a field record.

THE TEAM

Founding partners, board, advisors & auditors

Kronos is built by a bench of advanced-fuel-fusion, high-field-magnet, direct-conversion, and materials specialists, with a board and operations team drawn from defense, national laboratories, and industry. Dates are shown as ranges; where a tenure has ended or is term-ending, the range says so.

FOUNDING PARTNERS — SCIENCE

Dr. Gerald Kulcinski
Co-Founder · Helium-3 & Advanced-Fuel Fusion
UW–Madison · 2023–Present

Dr. Carl Weggel
Chief Scientist / S.M.A.R.T. Design
MIT Alcator Program · 2022–Present

Dr. Robert J. Weggel
Magnetic Field Design
MIT Magnet Lab · 2022–Present

BOARD

Priyanca Ford
Founder & CEO · Executive Board
2022–Present

Bandel Carano
Finance / Strategy
Oak Investment Partners / Stanford · 2025–2026

Patrick Schweiger
Fusion Device Engineering
Oklo / CFS / TerraPower · 2025–Present

SCIENTIFIC ADVISORS

Dr. Steven O. Dean
Fusion Policy & History
DOE / Fusion Power Associates · 2025–Present

Dr. Patrick H. Diamond
Plasma Turbulence & Transport
UC San Diego · 2025–Present

Dr. Jack J. Dongarra
HPC & Numerical Algorithms
Turing Award · 2025–Present

Dr. Nasr M. Ghoniem
Chief Material Scientist
UCLA · 2025–Present

Dr. Siegfried Glenzer
Plasma Physics & Laser Fusion
Stanford / SLAC · 2022–Present

Dr. David A. Hammer
Pulsed-Power Fusion
Cornell · 2025–Present

Dr. Donald A. Spong
Plasma Theory & Confinement
ORNL · 2025–Present

Dr. Curtis Smith
Risk Assessment & Nuclear PRA
MIT / Idaho National Lab · 2025–Present

RADM (Ret.) David Goggins
Naval Engineering & Power-Plant Design
U.S. Navy · 2023–2026

Dr. Konstantin Batygin
Mathematician
Caltech · 2022–2025

Dr. Ruben Fair
Magnet Design / ITER Liaison
PPPL / Jefferson Lab · 2022–2025

Dr. Paul S. Weiss
Materials & Nanotechnology
UCLA · 2022–2025

SCIENTIFIC AUDITORS

Dr. Wilfred A. Cooper
Plasma Equilibrium Theory
EPFL / Swiss Plasma Center · 2025–Present

Dr. Ahmed Hassanein
Plasma–Material Interactions
Purdue / Argonne · 2025–Present

Dr. Patrick E. Hopkins
Extreme Thermal Materials
U. of Virginia · 2025–Present

Dr. Peter Hosemann
Materials Joining & Structural Integrity
UC Berkeley · 2025–Present

Dr. Travis W. Knight
Advanced Nuclear Fuels & Systems
U. of South Carolina · 2025–Present

Dr. Philippe Lebrun
Cryogenics & Magnet Cooling
CERN · 2025–Present

Dr. Nitendra Singh
Nuclear Safety & Fuel Cycle
ITER · 2025–Present

Dr. Guido Van Oost
Magnetic Confinement & Fusion Systems
Ghent University · 2025–Present

Dr. Gary S. Was
Radiation Materials & Structural Integrity
U. of Michigan · 2025–Present

Dr. Ray Sedwick
Direct Energy Conversion
U. of Maryland · 2025

OPERATIONS

Michael Laughlin
Chief Operating Officer
2022–Present

Martin Owens
Chief Strategy Officer
LANL / GE Hitachi · 2022–Present

MG (Ret.) Paul Pardew
Chief Contracting Officer
Army Contracting Command · 2022–Present

David Beck
Fusion Commercialization
U.S. Space Force · 2024–Present

Sushma Bhatia
Environmental & Legislative
Google · 2022–Present

Michael De Frenza
Technology Licensing
2023–Present

MG (Ret.) Robin L. Fontes
Cybersecurity & Defense
Army Cyber Command · 2022–Present

Vijay Gehani
Supply Chain & Components
INOX India · 2024–Present

Jon Michel Greenwood
IT & AI Infrastructure
Live Nation · 2023–Present

Brian C. O'Neill
National Security
CIA / ODNI · 2022–Present

Gen. (Ret.) Gustave F. Perna
DoD Liaison
Operation Warp Speed · 2022–2023

Andrea Romero
Marketing Lead
2022–Present

Legal counsel is retained; those roles are held on the internal roster and are not listed here.

SOURCES

References

1 Y-K M Peng and D J Strickler, Features of spherical torus plasmas, *Nucl. Fusion* **26** 769 (1986).

2 M Ono *et al*, Exploration of spherical torus physics in the NSTX device, *Nucl. Fusion* **40** 557 (2000).

3 J E Menard *et al*, Fusion nuclear science facilities and pilot plants based on the spherical tokamak, *Nucl. Fusion* **56** 106023 (2016). doi:10.1088/0029-5515/56/10/106023

4 B N Sorbom *et al*, ARC: a compact, high-field, fusion nuclear science facility and demonstration power plant with demountable magnets, *Fusion Eng. Des.* **100** 378 (2015). doi:10.1016/j.fusengdes.2015.07.008

5 A J Creely *et al*, Overview of the SPARC tokamak, *J. Plasma Phys.* **86** 865860502 (2020). doi:10.1017/S0022377820001257

6 F Troyon, R Gruber, H Saurenmann, S Semenzato and S Succi, MHD-limits to plasma confinement, *Plasma Phys. Control. Fusion* **26** 209 (1984).

7 J Wesson, *Tokamaks*, 4th edn (Oxford: Oxford University Press, 2011).

8 J P Freidberg, *Plasma Physics and Fusion Energy* (Cambridge: Cambridge University Press, 2007).

9 ITER Physics Expert Group on Disruptions, Plasma Control and MHD *et al*, Chapter 3: MHD stability, operational limits and disruptions, *Nucl. Fusion* **39** 2251 (1999).

10 M Greenwald, Density limits in toroidal plasmas, *Plasma Phys. Control. Fusion* **44** R27 (2002). doi:10.1088/0741-3335/44/8/201

11 H-S Bosch and G M Hale, Improved formulas for fusion cross-sections and thermal reactivities, *Nucl. Fusion* **32** 611 (1992).

12 L L Lao, H St John, R D Stambaugh, A G Kellman and W Pfeiffer, Reconstruction of current profile parameters and plasma shapes in tokamaks, *Nucl. Fusion* **25** 1611 (1985). doi:10.1088/0029-5515/25/11/007

13 F Felici *et al*, Real-time physics-model-based simulation of the current density profile in tokamak plasmas, *Nucl. Fusion* **51** 083052 (2011). doi:10.1088/0029-5515/51/8/083052

14 M R Gilbert, S L Dudarev, S Zheng, L W Packer and J-Ch Sublet, An integrated model for materials in a fusion power plant: transmutation, gas production, and helium embrittlement under neutron irradiation, *Nucl. Fusion* **52** 083019 (2012). doi:10.1088/0029-5515/52/8/083019

15 D Stork *et al*, Developing structural, high-heat flux and plasma facing materials for a near-term DEMO fusion power plant, *Fusion Eng. Des.* **89** 1586 (2014).

16 R Prokopec, D X Fischer, H W Weber and M Eisterer, Suitability of coated conductors for fusion magnets in view of their radiation response, *Supercond. Sci. Technol.* **28** 014005 (2015).

17 A Sykes *et al*, First results from MAST, *Nucl. Fusion* **41** 1423 (2001).

18 M E Austin *et al*, Achievement of reactor-relevant performance in negative triangularity shape in the DIII-D tokamak, *Phys. Rev. Lett.* **122** 115001 (2019). doi:10.1103/PhysRevLett.122.115001

19 A Marinoni, O Sauter and S Coda, A brief history of negative triangularity tokamak plasmas, *Rev. Mod. Plasma Phys.* **5** 6 (2021). doi:10.1007/s41614-021-00054-0

20 O Sauter, C Angioni and Y R Lin-Liu, Neoclassical conductivity and bootstrap current formulas for general axisymmetric equilibria and arbitrary collisionality regime, *Phys. Plasmas* **6** 2834 (1999).

21 J Candy, E A Belli and R V Bravenec, A high-accuracy Eulerian gyrokinetic solver for collisional plasmas, *J. Comput. Phys.* **324** 73 (2016). doi:10.1016/j.jcp.2016.07.039

22 J Candy and R E Waltz, An Eulerian gyrokinetic-Maxwell solver, *J. Comput. Phys.* **186** 545 (2003). doi:10.1016/S0021-9991(03)00079-2

23 G M Staebler, J E Kinsey and R E Waltz, A theory-based transport model with comprehensive physics, *Phys. Plasmas* **14** 055909 (2007).

24 J Candy, C Holland, R E Waltz, M R Fahey and E Belli, Tokamak profile prediction using direct gyrokinetic and neoclassical

COLOPHON

How this document was made

The Kronos Fleet — Combined Editorial, 2026 is set in **Fraunces** (display), **Gelasio** (text), and **IBM Plex Mono** (data & equations), carried forward from the Kronos editorial design system.

The figures are rendered at 300 dpi from the deposited generator scripts; the document is composed as a single self-contained file with embedded fonts and imagery, paginated to US Letter, and rendered to PDF through a headless Chromium engine in matched light and dark editions.

Every headline quantity carries an evidence class; withdrawn and restated values are marked as such. Nothing herein is frozen beyond the founder-approved Tier-A set.

Explore it live — turn the interactive 3-D model, run the deposited solvers in the physics validator, and watch the companion film series.

LEGAL NOTICE

Notice, status, and distribution

Conceptual design & simulation study. This document reports a conceptual design and simulation study. It is not a construction commitment, a safety-analysis report, a regulatory filing, or an offer of securities. Forward-looking statements — schedules, costs, market sizes, and performance — are estimates subject to the limitations set out in the Simulations part and may change.

Numbers and their classes. Quantities are reported with evidence classes and case labels; modelled, assumed, and requirement-class values are identified as such and are not to be quoted without their labels.

Public edition. This edition carries the physics and design only; all financial, funding, and defense-commercial content has been removed for public distribution. The scientific text corresponds to the arXiv and journal submissions.

THE 2026 KRONOS SERIES

One programme, many papers

This editorial is one paper in the Kronos 2026 series — a real fusion company's complete, reproducible physics record for a spherical-tokamak breeder and its low-neutron D–^{3}He tandem-mirror burners. Every headline number is a frozen anchor in the Physics De-Risking Register.

Explore the whole programme: the De-Risking Register, the interactive 3-D model, and the physics validator.

KRONOS FUSION ENERGY

Lifetime-Constrained Operating-Window Synthesis for a Compact Spherical-Tokamak Breeder: The Source-Strength-Centrepost-Life Trade and the Admissible Current Window

A real fusion company building real machines. Explore the science, live.

Zenodo · doi:10.5281/zenodo.22645799

Read on kronosfusionenergy.com

The Physics De-Risking Register